

Carrier Trapping and Recombination: the Role of Defect Physics in Enhancing the Open Circuit Voltage of Metal Halide Perovskite Solar Cells

Tomas Leijtens^{1,2}, Giles E. Eperon³, Alex J. Barker¹, Giulia Grancini¹, Wei Zhang³, James M.
Ball¹, Ajay Srimath Kandada¹, Henry J. Snaith³, Annamaria Petrozza^{1*}*

¹Center for Nano Science and Technology @Polimi, Istituto Italiano di Tecnologia, via Giovanni
Pascoli 70/3, 20133, Milan, Italy

²Department of Materials Science and Engineering, Stanford University, Stanford, CA 94305

³University of Oxford, Clarendon Laboratory, Parks Road, Oxford, OX1 3PU, United Kingdom

Abstract

One of the greatest attributes of metal halide perovskite solar cells is their surprisingly low loss in potential between bandgap and open-circuit voltage, despite the fact that they suffer from a non-negligible density of sub gap defect states. Here, we use a combination of transient and steady state photocurrent and absorption spectroscopy to show that $\text{CH}_3\text{NH}_3\text{PbI}_3$ films exhibit a broad distribution of electron traps. We show that the trapped electrons recombine with free holes unexpectedly slowly, on microsecond time scales, relaxing the limit on obtainable Open-Circuit Voltage (V_{oc}) under trap-mediated recombination conditions. We find that the observed V_{oc} s in such perovskite solar cells can only be rationalized by considering the slow trap mediated recombination mechanism identified in this work. Our results suggest that existing processing routes may be good enough to enable open circuit voltages approaching 1.3 V in ideal devices with perfect contacts.

28 **Introduction**

29 Metal halide perovskite solar cells owe their rapid rise to power conversion efficiencies
30 over 22 %^{1,2} to several key properties. They benefit from their low exciton binding energies^{3,4},
31 high ambipolar mobilities⁵⁻⁷, high absorption cross-sections⁸, and long carrier lifetimes⁹⁻¹¹.
32 These properties have allowed this class of materials to function effectively as not just
33 photovoltaic devices, but also as light emitting diodes (LEDs) and optically pumped lasers¹²⁻¹⁴.
34 Still, the materials are known to suffer from a significant density of sub gap states that should
35 induce non-negligible recombination losses^{10,11,15,16}. Extensive time resolved photoluminescence
36 and terahertz spectroscopy on the most commonly employed CH₃NH₃PbI₃ perovskite has shown
37 that at solar fluences, the photo-carrier dynamics are limited by a monomolecular trapping
38 process while the radiative bimolecular recombination process is surprisingly slow and hence
39 only dominates at high excitation densities^{7,10,11,17}. While it is accepted that carrier trapping plays
40 a dominant role in perovskite photo-carrier dynamics at solar fluences, the nature of the traps and
41 the recombination pathway has remained unexplored.

42 Generally, carrier trapping into deep subgap states is considered to lead to rapid non-
43 radiative recombination which severely limits the quasi-Fermi level splitting of the materials,
44 and hence photovoltage of the solar cells. This follows the Shockley Reed Hall (SRH)
45 framework, where recombination occurs through a state within the forbidden band of the
46 semiconductor. SRH behavior can be categorized by two distinct regimes where the
47 semiconductor is either doped or closer to intrinsic. In a highly doped semiconductor, trapping
48 into a sub gap state leads to immediate annihilation by the many excess carriers of the opposite
49 charge, while trapping into such a state does not necessarily lead to immediate recombination in
50 a lightly or undoped material. The SRH model has generally been applied to highly doped silicon

51 solar cells where trapping results in immediate recombination and hence the trapping lifetime of
52 the minority carrier becomes the most relevant parameter¹⁸. Indeed, SRH recombination has been
53 generally proposed to dominate in lead halide semiconductors^{7,11,18,19}. Despite evidence that the
54 perovskite layers are generally only lightly doped, past work has primarily assumed that the
55 recombination rate of the trapped electron or hole is the same as the trapping rate, and hence the
56 trapping lifetime has been used to estimate both electron and hole diffusion lengths^{6,7,20}. With the
57 reported sub-gap trap densities of around 10^{16} cm^{-3} and an effective trapping lifetime of about
58 $100 \text{ ns}^{10,11}$, rapid trap mediated recombination would result in a severe limitation in attainable
59 photovoltages of perovskite solar cells. Still, this relatively new technology boasts voltages
60 already approaching $1.2 \text{ V}^{21,22}$, which is remarkably high for a semiconductor with a bandgap of
61 only 1.6 eV . In the limit where all recombination is due to radiative band-to-band recombination
62 the material should be able to achieve ideal V_{OCs} around 1.3 V^{23} , not much higher than what has
63 been already experimentally obtained. This suggests that the subgap states, thought to be almost
64 unavoidable in a solution processed and low-temperature crystallized material, may not form
65 highly detrimental recombination centers. Previous photoconductivity measurements led us to
66 suggest that the carrier trapping process leads to a photodoping effect, which implies a long lived
67 trapped species and associated long lived free carrier species¹⁵. Such slow trap mediated
68 recombination would allow for far greater fermi level splitting and V_{OCs} compared to rapid trap
69 mediated recombination where the trapped carriers recombine almost instantaneously with free
70 carriers. Still, such a phenomenon has hitherto remained unexplored within the field of
71 perovskite solar cells. While several photophysical models have been developed to explain
72 photoluminescence decays^{7,10,11}, none have been extended to consider the recombination
73 lifetimes of the trapped charge even though this may be one of the most relevant parameters to

74 consider when it comes to determining how detrimental a given density of trap sites might be to
75 the total recombination flux, quasi fermi level splitting, and photovoltage in solar cells. Some
76 important questions that remain to be addressed can be summarized as follows: 1) do the
77 predominant defects act as electron or hole traps? 2) what is their energetic distribution? 3) how
78 rapid is trap mediated recombination? 4) how does the effective carrier lifetime affect the
79 theoretically obtainable V_{OCs} of perovskite solar cells?

80 In this work, we directly monitor trapped electron – free hole recombination kinetics in
81 metal halide perovskite films for the first time, establishing that $CH_3NH_3PbI_3$ suffers from a
82 significant and broad density of sub gap electron traps. Surprisingly, after an initial fast electron
83 trapping process (100 ns lifetime), the trapped electrons slowly recombine with free holes on
84 tens of μs timescales, thus deviating significantly from the expected rapid trap mediated
85 recombination pathway. This results in a situation where most of the traps are filled at solar
86 fluences allowing the solar cells to obtain improved photovoltages.

87 We finally address the implications to the theoretically obtainable V_{OCs} in perovskite
88 solar cells by using simple Fermi-Dirac statistics. If we account for the slow trapped charge
89 recombination and associated trap filling we estimate maximum obtainable V_{OCs} close to 1.3V,
90 about 150 mV higher than that expected for rapid trap mediated recombination — clearly more
91 consistent with the experimental results^{21,22}. These findings shed light on the high photovoltages
92 achieved for this system despite the inevitable presence of significant trap densities inherent in
93 solution processed semiconductors.

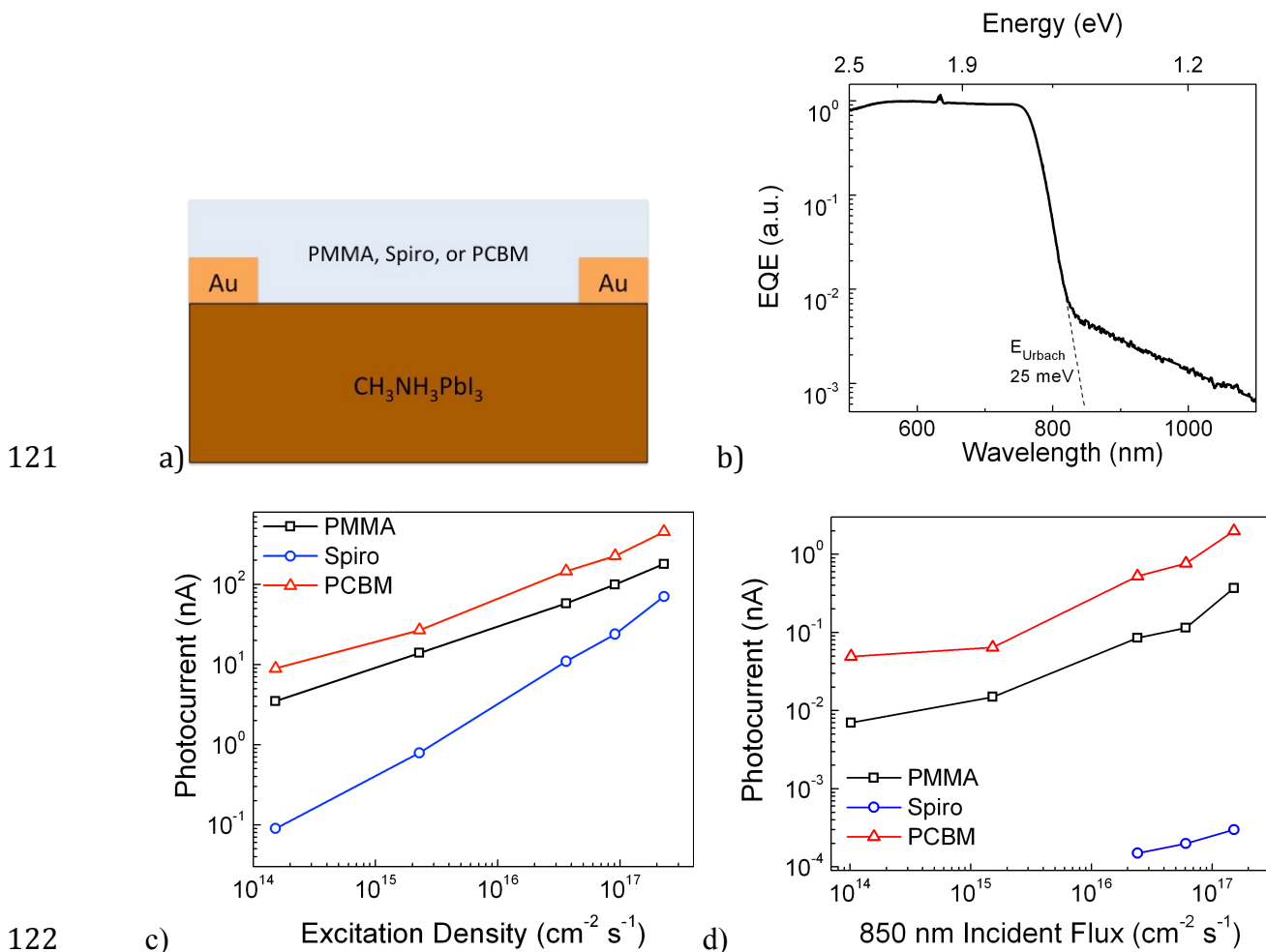
94 **Results and Discussion**

95 **1. Nature and energetic distribution of trap sites**

96 In order to firstly measure the trap energy distribution, we performed Fourier transform
97 photocurrent spectroscopy on a perovskite layer with two lateral ohmic contacts, which serves as
98 a photoresistor. Any photocurrent collected upon sub gap excitation directly implies the presence
99 of sub gap sites, and so this measurement allows us to obtain the energetic distribution of such
100 states.

101 The sample structure is shown in **Figure 1a**, and the normalized photocurrent spectrum is
102 shown in **Figure 1b**. We used a gold/perovskite/gold structure (the perovskite deposition
103 method for all measurements except where otherwise noted is the PbCl_2 derived perovskite)
104 which guarantees an ohmic response limited by the semiconductor layer rather than the contacts
105 (see Figure S1)^{24,25}, applying a bias of 10 V over a channel of 4 mm. Since the device functions
106 as a planar photodetector with symmetric contacts, we only require the presence of one free
107 carrier to measure any photocurrent under external applied bias¹⁵. This allows us to detect
108 transitions that result in only one free carrier, such as a direct valence band to trap level
109 transition. Consistent with previous reports of low Urbach energies we observe a sharp band
110 edge onset in the photocurrent corresponding to an Urbach energy of 25 meV²⁶ (Fig. 1), but also
111 observe an additional broad tail with a distinct slope in the photocurrent extending from the band
112 edge to the instrument limitation at almost 1.1 eV. This is direct evidence for the presence of a
113 broad distribution of trap states down to at least 0.5 eV from either the valence or conduction
114 band edge. Previous theoretical studies have focused on identifying distinct types of defects with
115 discrete energy levels, with the most recent work suggesting that iodide interstitials are likely to
116 manifest themselves as relatively deep electron traps²⁷⁻²⁹. The shape of our subgap photocurrent
117 spectrum is not completely coherent with this scenario. It seems possible that the broad
118 distribution of subgap states could be due to an inhomogeneity in crystallinity and perhaps

119 stoichiometry on the nano-to-micro scale, or even to the presence of multidimensional defects
 120 which have not yet been well studied.



123 **Figure 1.** (a) Schematic of the symmetric laterally contacted device held under 10 V applied bias. (b)
 124 Normalized photocurrent spectral response of the device at an applied bias of 10 V. the device is
 125 encapsulated with an inert PMAA layer. (c) Photocurrent (10 V) as a function of intensity of an above gap
 126 (690 nm) excitation for devices covered by a hole accepting Spiro-OMeTAD, an electron accepting
 127 PCBM, or an inert PMMA layer. (d) Photocurrent (10 V) of the same devices as a function of fluence of a
 128 sub gap (850 nm) excitation. We point out that the fluence denoted in 1d is not equivalent to an absorbed
 129 fluence; the absorption cross-section at 850 nm is unknown and may be different for the different
 130 samples.

131

132 Having established that our material is suffering from the presence of a broad distribution
133 of sub gap trap sites, we aim to determine whether this distribution is associated with electron or
134 hole trapping, or both. Here, we measure the photocurrent from the same device architecture
135 shown in Fig 1.a upon monochromatic excitation both above and below gap. We compare the
136 pristine perovskite covered by a thin layer of inert PMMA with one covered by a thin hole
137 accepting (spiro-OMeTAD, referred to as Spiro), or electron accepting layer (PCBM)⁵. The
138 perovskite is directly excited and the vast majority of the detected current comes from the
139 carriers in the perovskite layer only (see supplemental discussion S1)¹⁵. We point out that the
140 photocurrent measured here is proportional to the carrier densities and their mobilities. Under
141 steady state illumination, the carrier density is determined by the carrier lifetime. This can be
142 formally represented by **Equation 1**³⁰:

143

$$144 \quad I \propto q(n \cdot \mu_n + p \cdot \mu_p) = q(G \cdot \tau_n \cdot \mu_n + G \cdot \tau_p \cdot \mu_p) \quad \text{Eq. 1}$$

145

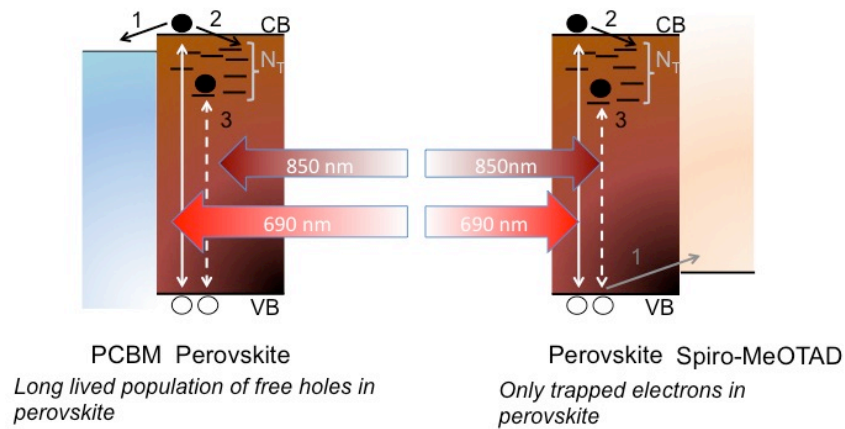
146 where I is the photocurrent, q is the elemental charge, n and p the electron and hole densities
147 respectively, μ the carrier mobilities, G the generation rate, and τ the effective carrier lifetimes at
148 the relevant conditions. Considering that PCBM and Spiro have been previously demonstrated to
149 be effective electron and hole acceptors⁵, reducing PL by over 90 %, it is fair to consider only
150 hole densities and mobilities within the perovskite in presence of the PCBM acceptor and only
151 electron densities and mobilities in presence of the Spiro acceptor. The results obtained upon
152 above gap excitation are displayed in **Figure 1c**. The steady state photocurrent in samples with
153 PCBM electron accepting layers is higher than that of samples with an inert top layer. This is

154 expected, since electron transfer to PCBM will result in a longer lived free hole population in the
155 perovskite. Lifetime will be associated with the recombination rate between a hole in the
156 perovskite and an electron in the PCBM layer. Such lifetimes have been found to be on the order
157 of 1-10 μ s via transient photovoltage measurements for recombination at both the perovskite-
158 PCBM and perovskite-Spiro interfaces³¹. Surprisingly, the samples with the Spiro hole acceptor
159 exhibit orders of magnitude lower photocurrent even than the neat samples, despite the fact that
160 they should also exhibit enhanced lifetimes associated with slow recombination across the
161 perovskite-Spiro interface (electrons in perovskite with holes in Spiro). This leads us to conclude
162 that either the electron mobility is orders of magnitude lower than the hole mobility, or that
163 electrons are predominantly trapped. Since the effective masses for electrons and holes has been
164 repeatedly shown to be roughly the same^{3,32,33}, we believe that our results indicate that electrons
165 are trapped and hence suffer from a low *effective long range* mobility.

166 So far, the results suggest that the material suffers from a significant and broad density of
167 sub gap electron traps, which limit the effective long-range electron mobility. To relate the
168 photo-current response upon sub gap excitation observed in Figure 1b to the behavior in Figure
169 1c, we excite the samples with a sub gap excitation source (850 nm laser) and monitor the
170 photocurrent. The results are plotted in Figure 1d, and show that sub gap excitation leads to little
171 to no detectable photocurrent (over three orders of magnitude lower than the neat samples) when
172 a hole acceptor is placed on top of the samples. On the other hand, the presence of an electron
173 acceptor has a similar effect as with above gap illumination. This allows us to claim that deep
174 electron traps are present, which can be directly populated by excitation from the valence band to
175 yield trapped electrons and free holes. The free holes can be collected as photocurrent in neat
176 samples, but no photocurrent is collected in samples with the Spiro hole acceptor simply because

177 there are only trapped electrons left in the film. The proposed mechanism is displayed in Scheme
 178 1. It is worth noting that upon sub-gap excitation, in principle, one would expect the same photo-
 179 current for PCBM and PMMA contacted thin films. Nevertheless in Figure 1d we can notice a
 180 small deviation. We speculate that this may be due to a different chemical interaction between
 181 the interfaced materials which may cause the density, nature, distribution, and lifetime of trapped
 182 electrons to be different.

183



184

185

186 **Scheme 1.** Schematic illustration of carrier dynamics upon above and below gap excitation when the
 187 perovskite is contacted by electron (PCBM) and hole (Spiro-MeOTAD) accepting layers.

188 Note that in Figure 1c, the sublinear behavior for the electron-accepting sample suggests
 189 that recombination across the perovskite-PCBM interface has a charge density dependence,
 190 while this is not observed for the perovskite-Spiro interface. This is well in agreement with the
 191 scenario where free electrons in the PCBM and free holes in the perovskite recombine in the first
 192 case, while free holes in the spiro will recombine with localized, trapped electrons in the
 193 perovskite in the second case.

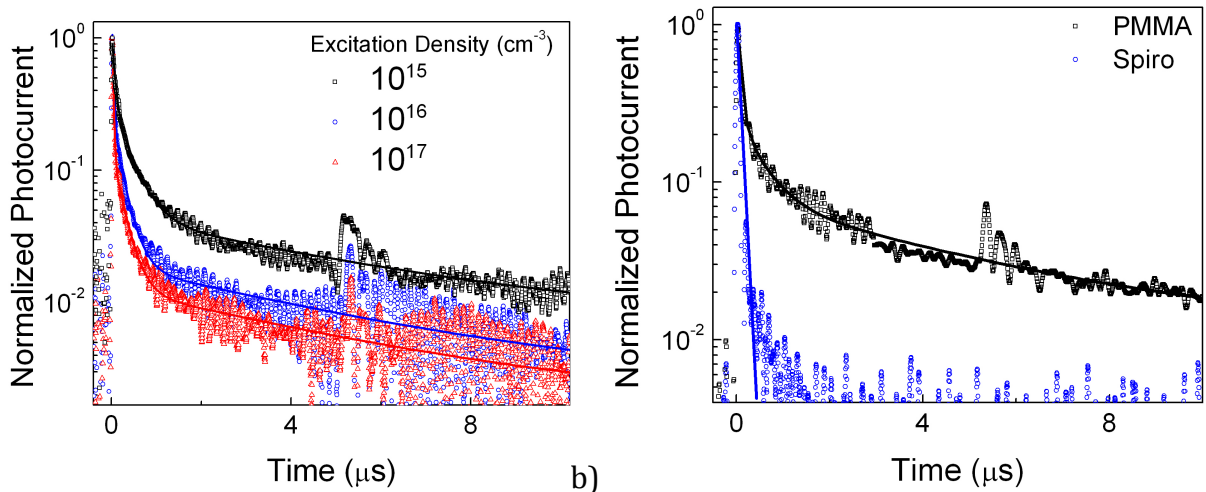
194 **2) Trap mediated recombination lifetimes and mechanism**

195 In an effort to directly monitor the trapped electron lifetimes, we performed transient
196 photocurrent measurements on the same samples used for the steady state photocurrent
197 measurements, this time using a pulsed excitation analogous to that used in transient PL
198 measurements rather than a steady state excitation. This measurement allows us to monitor the
199 transient photoconductivity of the perovskite layer with various charge quenching layers, and
200 thus directly probe the free carrier population as a function of time after excitation. Monitoring
201 the photoconductivity rather than the photoluminescence means that we are not limited by the
202 presence of radiative recombination but can monitor any free carrier. We start by performing an
203 above gap fluence dependence with non-quenching samples (Figure 2a). At early times ($< 1 \mu\text{s}$)
204 the decays become steeper for higher excitation densities as previously observed via
205 photoluminescence spectroscopy when moving from monomolecular to bimolecular
206 recombination regimes. Interestingly, we also observe an extremely slow component in the
207 photoconductivity traces that makes up an increasingly large fraction of the decay as the
208 excitation density is reduced. This component has not generally been observed in transient
209 photoluminescence data we and others^{7,10,11,20,34} have ever recorded for $\text{CH}_3\text{NH}_3\text{PbI}_3$ (see Figure
210 S2), which means that whichever mobile photoexcited species is still present on these long time
211 scales cannot relax radiatively. It is reminiscent, however, of some of the slow decays observed
212 when measuring transient voltage decays³⁵. Notably this slow component, which appears to
213 decrease in decay rate over time, makes up less than 10 % of the total decay upon high excitation
214 (10^{17} cm^{-3}) but approximately 50 % of the total decay upon low (10^{15} cm^{-3}) excitation. Since the
215 signal is directly proportional to the photoconductivity and hence carrier density, its relative
216 magnitude is used as a proxy for carrier density.

217 We performed the same measurements (at ‘low’ 10^{15} cm^{-3} excitation density) for a
218 sample with the hole layer (Figure 2b). It shows an extremely rapid decay in the photocurrent
219 and do not show any observable slow tail, unlike for the case of the PMMA and PCBM (see
220 Figures S2 and S3) covered samples. This decay is consistent with rapid hole transfer to the
221 Spiro⁵, leaving only electrons in the material, which clearly do not contribute to any photocurrent
222 on time scales > 10 s of ns. As evidenced by both these and the steady state photocurrent
223 measurements in Figure 1, it is evident that the electrons do not contribute to any significant
224 photocurrent, at least for long-range transport. This is direct proof that electrons are
225 predominantly being trapped in the $\text{CH}_3\text{NH}_3\text{PbI}_3$ perovskite with ~ 100 ns monomolecular
226 lifetimes.

227 We can now explain the fluence dependent transient photocurrent kinetics for the neat
228 samples shown in Figure 2a. As the excitation density approaches the trap density, the slow
229 component takes up an increasingly large fraction of the decay. At low excitation densities, most
230 of the generated electrons are trapped on 100s of ns timescales as has been previously reported
231 for these materials and as we show here (see fits in Figure S4), and free holes are left behind
232 until they recombine with the trapped electrons. These holes are responsible for the remaining
233 slowly decaying photocurrent. The fact that the slow component of the decay takes up a large
234 fraction of the decay only once initial densities of 10^{15} cm^{-3} are used means that the trap density
235 lies somewhere between 10^{15} - 10^{16} cm^{-3} , similar to what we have previously found from
236 photoluminescence decays in these materials^{10,11}. While a rapid trap mediated recombination
237 model would suggest that once the electrons are trapped, they should recombine at a similar rate
238 with free holes, our data shows that this recombination process is actually extremely slow and
239 takes place via a density dependent process that can be as slow as many microseconds. This is

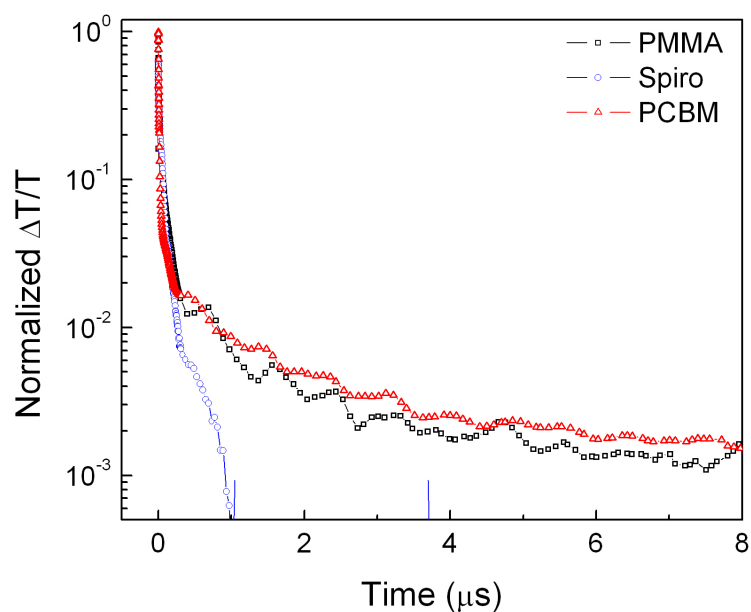
240 more akin to the situation in materials such as ZnO or TiO₂ where holes can be trapped at
241 surfaces for long times of up to seconds, leaving free electrons^{36,37}. This is known as a
242 “photodoping” effect, which is what we propose to be happening in our perovskite thin films.
243 Since the material is ionic and defects are expected to be charged^{27,38,39}, a filled trap is likely to
244 be neutral and hence relatively unlikely to lead to rapid recombination.



245 a) 246 **Figure 2.** (a) Transient photocurrent (20 V) of a device upon 690 nm excitation at three different
247 excitation densities. The device is covered with just an inert PMMA layer. (b) Transient photocurrent (20
248 V) traces for devices with the hole accepting Spiro and the inert PMMA layers, measured at 690 nm at
249 10¹⁵ cm⁻³ excitation densities.

250 If such an effect is observable via the photoconductivity across thin films, it should also
251 be observable in transient absorption kinetics. Indeed, since the long lived photoconductivity in
252 neat samples and samples with PCBM electron acceptor represents the presence of a long lived
253 free hole population, this should be observable as a bleach at the perovskite band edge due to
254 state filling in the valance band⁴⁰. We therefore performed transient absorption studies on neat
255 films and films with PCBM and Spiro accepting layers. We display transient absorption decays
256 probed at the peak of the band edge bleach at 750 nm in **Figure 3**. The high initial excitation
257 density (necessary to detect the small long lived signal) results in rapid initial decay,

258 corresponding to bimolecular recombination in the PMMA coated samples and to a combination
259 of bimolecular recombination and charge transfer for the Spiro and PCBM coated samples. Still,
260 by measuring the decay to longer time scales than have been previously reported, we find that
261 the transient absorption decays closely mimic the transient photocurrent decays, exhibiting a
262 significant long-lived free carrier population only in presence of PMMA and PCBM, which we
263 can now assign to remnant free holes in the valence band. Of course, this implies that hole
264 diffusion lengths in perovskite films are likely to be much longer than electron diffusion lengths.



265
266 **Figure 3.** Transient absorption decay probed at 750 nm for sample coated with PMMA, PCBM, and
267 Spiro. The excitation wavelength was 532 nm at 10^{18} cm^{-3} initial excitation density. A zoomed in version
268 of the long living tails is plotted on a linear scale in Figure S5.

269 The fact that recombination of the trapped electrons with free holes is extremely slow has
270 significant implications to perovskite solar cells. Since the balance between the generation and
271 recombination rates of trapped carriers determines their depopulation, the slower the
272 depopulation rate, the lower the illumination intensity required to fill all the trap states at steady
273 state. This effect would in principle increase the expected V_{OC} value at a fixed density of trap

274 states, since the total non-radiative recombination rate will be lower, enabling operation closer to
275 the radiative limit.

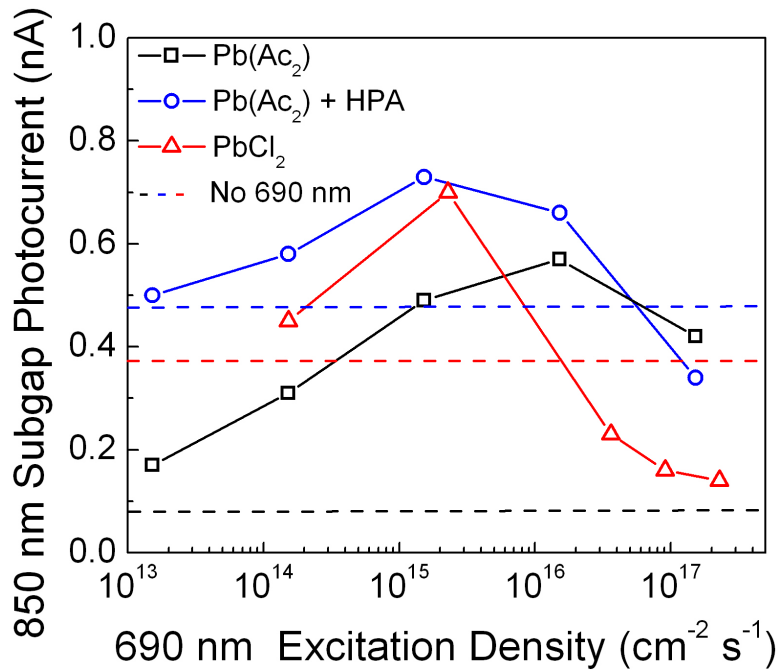
276 To further quantify steady state trap filling, we have taken films formed via different
277 preparation routes and hence likely with different trapping rates and densities, and studied the
278 illumination intensity at which the traps are primarily filled. To accomplish this, we monitor the
279 photocurrent contribution from a modulated sub-gap excitation (850 nm) as a function of a
280 steady-state above-gap excitation (650 nm). We modulate only the 850 nm laser and use a lock-
281 in amplifier to detect the photocurrent signal from this modulation. Based on the discussion
282 above, we expect to observe a point at which the above gap excitation background has filled
283 most of the trap sites, and the subgap contribution should shrink. The background fluence at
284 which the subgap contribution becomes less than it was in the absence of any above gap
285 excitation background gives an idea of the illumination intensity required to fill the traps at
286 steady state and achieve optimum fermi level splitting.

287 We have chosen to use three MAPbI₃ preparation routes which we have previously
288 optimized to provide efficient devices: the PbCl₂ derived perovskite, the Pb(Ac)₂ derived
289 perovskite⁴¹, and the Pb(Ac)₂ perovskite treated with hypophosphorous acid (HPA)⁴². These
290 routes provide a wide range of crystal sizes (see SEM images in Figure S6), with the Pb(Ac)₂
291 route giving the smallest small crystals, HPA-treated Pb(Ac)₂ increasing the crystal size
292 somewhat, and the PbCl₂ route having the largest crystals^{42,43}.

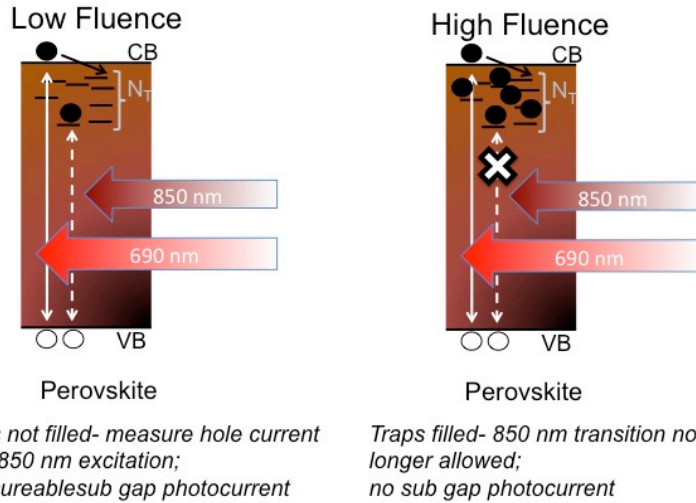
293 We show the measurements of subgap photocurrent in **Figure 4**, where the HPA treated
294 sample demonstrates significant trap filling at $1.7 \times 10^{17} \text{ cm}^{-2} \text{ s}^{-1}$, but the non HPA treated
295 Pb(Ac)₂ derived film demonstrates a less significant trap filling at equivalent fluences.
296 Interestingly, the PbCl₂ derived perovskite gives evidence for the most quick trap state filling,

297 with the IR photocurrent contribution diminishing at a fluence of $2 \times 10^{16} \text{ cm}^{-2} \text{ s}^{-1}$. Again, this is
298 established by the above gap excitation fluence at which the IR photocurrent is rapidly declining
299 and drops below what it was in the absence of any above gap excitation.

300 The results indicate that of the three perovskite routes, the PbCl_2 route may be the most
301 favorable in terms of achieving a material with low trap densities. However, it has been
302 notoriously difficult to obtain films with 100 % coverage of the substrate⁴⁴, resulting in pinholes
303 and losses in open circuit voltages. This has led to the use of the $\text{Pb}(\text{Ac})_2$ derived perovskite,
304 which forms into extremely smooth and continuous films. However, this appears now to come at
305 the price of a slightly increased trap density. This points to traps being localized predominantly
306 on the surface of crystals, since this route attains smaller grains sizes^{42,43}. The HPA treatment
307 still allows for the formation of smooth and continuous films, but clearly seems to decrease the
308 trap density and result in a material in which most of the traps are filled, consistent with a slight
309 increase in grain size (though not to the extent of the PbCl_2 films).



310



311 *Traps not filled- measure hole current from 850 nm excitation; measurable sub gap photocurrent*

312 **Figure 4.** The subgap photocurrent contribution is monitored as a function of above gap light excitation

313 fluence for devices coated with PMMA. The perovskite films are derived from the $\text{Pb}(\text{Ac})_2$ route (with

314 and without HPA treatment) and PbCl_2 routes. The sub gap contribution is distinguished by modulating

315 the 850 nm and using a lock in amplifier to detect only this signal. The dashed lines represent the sub gap

316 photocurrent contribution in the absence of any above gap photoexcitation bias. The solid lines are simply

317 to guide the eye, while the data points are denoted by symbols. b) Schematic demonstrating the sub gap

318 current generation mechanisms at low and high fluences.

319 The most significant behavior observed here is that the different samples exhibit very

320 different points at which their sub gap contribution is strongly diminished, consistent with

321 varying trapping and trapped electron – hole recombination rates. We confirm this again by

322 plotting the transient photocurrent of $\text{Pb}(\text{Ac})_2$ -derived perovskite films with and without HPA in

323 Figure S7, where we find that that the HPA treatment slows the trapped electron – hole

324 recombination rate as well as the trapping rate itself. This is further evidence that the absolute

325 trap density and processing route of the films affects the rate at which trapped electrons can

326 recombine with free holes, and that not all traps behave the same. Of course, this was already

327 expected from the broad distribution of sites exhibited in Figure 1b.

328 **Implications to V_{OC}**

329 We can take this analysis slightly further, and estimate the obtainable photovoltage due to
330 the effectiveness of fermi level splitting, bearing in mind what we have learned from the
331 measurements presented here. If the 100 ns (taken as a typical value for many of the perovskite
332 films used throughout different laboratories)^{6,20,21} electron trapping process resulted in immediate
333 recombination of the trapped electron with a free hole, the effective electron and hole lifetimes
334 would both be 100 ns. Of course, if the trapped electron to free hole recombination rate is
335 extremely slow then it is likely many traps can be filled at solar fluences (as is the case for the
336 PbCl₂ derived and HPA treated Pb(Ac)₂ derived perovskite films), high hole densities are
337 reached, and only the radiative bimolecular recombination rate becomes increasingly relevant.
338 Using the simple relations shown below⁴⁵, it is possible to estimate the maximum obtainable
339 fermi level splitting and hence a rough approximation of maximum V_{OC} for the three cases: rapid
340 100 ns trap mediated recombination, a slow trap mediated recombination model, vs complete
341 trap filling at 1 sun and resultantly only bimolecular recombination;

$$342 \quad G = R(n, p) \quad (2)$$

$$343 \quad R(n, p)_{mono} = \frac{n}{\tau} = \frac{p}{\tau} \quad (3)$$

$$344 \quad R(n, p)_{bimol} = n \cdot p \cdot B \quad (4)$$

$$345 \quad V_{OC} = E_{Fn} - E_{Fp} = E_G - KT \cdot \ln\left(\frac{n}{N_C}\right) - KT \cdot \ln\left(\frac{p}{N_V}\right) \quad (5)$$

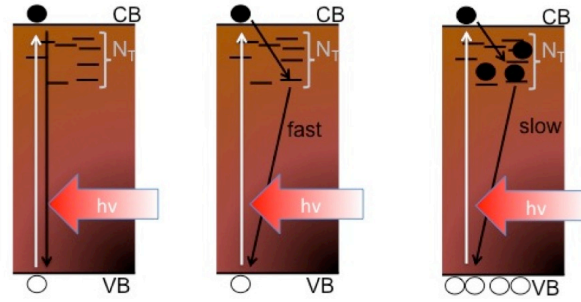
346
347 where G is the generation rate (based on J_{SC} of 23 mA cm⁻² and a 500 nm thick film), $R(n, p)$ is
348 the recombination rate of electrons and holes respectively, τ is the monomolecular recombination
349 lifetime, B is the bimolecular recombination coefficient (9 x 10⁻¹⁰ cm⁻⁹ s⁻¹), E_{Fn} and E_{Fp} are the
350 quasi fermi levels for electrons and holes respectively, E_G is the bandgap (1.6 eV), KT is the
351 thermal energy in eV, and N_C (1.9 x 10¹⁸ cm⁻³) and N_V (2.4 x 10¹⁸ cm⁻³) are the effective density

352 of states of the conduction and valence bands respectively. We calculate the effective density of
 353 states based on the reported electron and hole effective masses of approximately 0.18 and $0.21m_0$
 354 for electrons and holes respectively^{3,32}. Here, we simply estimate the steady state carrier densities
 355 based on the rate equations shown above for the different cases: for the first case we assume a
 356 100 ns monomolecular lifetime for both electrons and holes, for the second case we assume a
 357 100 ns lifetime for electrons but a 10 us lifetime for holes, and for the third case we simply use
 358 the literature value for the bimolecular recombination coefficient and calculate the corresponding
 359 electron and hole densities at one sun's worth of excitation. Once the carrier concentrations are
 360 known, we can use the calculated density of states to determine the degree of quasi fermi level
 361 splitting for each type of carrier. Table 1 shows our estimation of electron and hole densities as
 362 well as the resultant Fermi level splitting and theoretically obtainable V_{OC} s for the two extreme
 363 cases. We also describe the situation where electron traps are not filled but the trapped electron
 364 to free hole recombination has a slow monomolecular lifetime of 10 μ s (a conservative
 365 approximation based on the transient decays shown in Figure 2 and 3).

366 **Table 1.** Electron (n) and hole (p) densities, corresponding fermi level splitting, and theoretical V_{OC} s for
 367 the three different dominant recombination mechanisms described in Scheme 2.

	G ($\text{cm}^{-3} \text{s}^{-1}$)	n (cm^{-3})	p (cm^{-3})	$ E_C - E_{Fn} $ (eV)	$ E_V - E_{Fp} $ (eV)	V_{OC} (V)
100 ns trap recombination	2.9×10^{21}	2.9×10^{14}	2.9×10^{14}	0.23	0.23	1.14
Traps Filled- bimolecular	2.9×10^{21}	5.7×10^{15}	5.7×10^{15}	0.15	0.16	1.30
Long Lived Holes	2.9×10^{21}	2.9×10^{14}	2.9×10^{16}	0.23	0.11	1.26

368



Traps filled Bimolecular Trapping - fast Trapping – long lived holes

369

370 **Scheme 2.** The three different recombination mechanisms considered in Table 1 are schematically
 371 illustrated.

372 This analysis makes it very clear that a rapid trap mediated recombination model with
 373 100 ns trapping and recombination lifetimes would lead to very low electron and hole densities
 374 yielding low theoretical V_{OC} s of approximately 1.14 V, which is incompatible with the high
 375 experimental observed values of up to 1.19 V²¹. We note that we ignore recombination across the
 376 ETL and HTM interfaces with the perovskite, and that the values presented here are very clearly
 377 the maximum attainable values assuming ideal contacts. When we consider the results from
 378 Figure 4 which indicate that traps are starting to be filled for the PbCl₂ derived material, we must
 379 consider the situation where primarily bimolecular recombination affects the carrier dynamics
 380 and densities, or at least a situation where most traps are filled and hence the behavior is more
 381 akin to the bimolecular case. The photoluminescence quantum yields of perovskite films made in
 382 this way have been reported to be 10-30 %^{10,13} at solar fluences, which is in line with a situation
 383 where most, but likely not all, traps are filled. In a perovskite film with traps filled, where
 384 bimolecular recombination is the dominant mechanism, it becomes possible to obtain high V_{OC} s
 385 of approximately 1.3 V in line with the thermodynamic limit for a 1.6 eV semiconductor, and
 386 consistent with the highest reported values of 1.19 V in a real device. Considering the situation
 387 where traps are further from completely filled, like the case for the Pb(Ac)₂ derived perovskite,

388 but including the fact that trapped electrons only recombine with free holes on slow (μs)
389 timescales, we find that it is possible to obtain high V_{OCs} of approximately 1.26 V, still
390 consistent with the high observed voltages even in non optimized films with significant electron
391 trap densities. In this case, the high hole densities obtained at one sun's worth of excitation mean
392 that radiative recombination will start to compete with the trapping process, i.e. the extremely
393 slow hole recombination will result in increasingly high PLQEs even at low fluences such as at
394 one sun. We make a rough estimation of the relative contribution due to radiative recombination
395 for the fast and slow trap mediated recombination (scenario 1 and 2 in the table) and find that
396 this yields photoluminescence quantum yields of 0.3 and 26 %, respectively. This analysis
397 proves that it is not possible to obtain high quantum yields nor high fermi level splitting in our
398 perovskite materials if we simple consider 100 ns trapping and recombination time constants. In
399 fact, we now find that the reported quantum yields of 10-30% is only well explained by the fact
400 that trapped carriers are long lived, allowing high enough carrier densities to be reached to
401 facilitate radiative recombination even at one sun. We note that our estimations ignore any non-
402 radiative recombination due to the introduction of the selective contact layers or even other
403 deeper traps through which recombination may be more rapid which we cannot identify here.
404 The charge selective contacts have been shown to limit the ELQE and PLQE of perovskite
405 devices⁴⁶, and thus currently present a severe limitation on the obtainable photo voltages in solar
406 cells. However, our results show that as the contacts continue to improve, we can expect to
407 observe V_{OCs} approaching 1.3 V without any need for further improvement in optoelectronic
408 quality of the perovskite films themselves.

409 **Conclusions**

410 We have used a combination of transient and steady state photocurrent, absorption, and
411 photoluminescence spectroscopy to study the carrier dynamics in perovskite films over long time
412 scales. Electron trapping is a predominant decay pathway, but the trapped electrons are
413 surprisingly long lived; they only recombine with associated free holes over the course of many
414 microseconds. This allows most of the traps in perovskite films made with typical deposition
415 methods to be filled at solar fluences and hence allows us to rationalize the high V_{OCs} reported
416 for perovskite solar cells, which exceed the limits imposed by a rapid trap mediated
417 recombination model. We furthermore find that due to these fortuitously long lived traps,
418 perovskite films made via existing processing routes exhibit or are close to exhibiting high
419 enough optoelectronic quality that they should enable solar cells with V_{OCs} approaching 1.3 V
420 provided that non radiative decay due to contact layers can be mitigated.

421

422 **Experimental Section**

423 *Perovskite fabrication method*

424 Glass substrates were sequentially cleaned in Helmanex soap, acetone, and isopropanol. Most of
425 the measurements (unless otherwise noted) were performed on perovskite films made via the
426 $PbCl_2$ precursor method. Here, 0.8M solutions of 3:1 (by molar concentration) of
427 methylammonium Iodide: $PbCl_2$ in DMF were spin coated on oxygen plasma cleaned glass
428 substrates at 2000 rpm for 45 seconds in a nitrogen filled glovebox. The substrates were allowed
429 to dry at room temperature for 30 minutes, then annealed at 90 C for 90 minutes, followed by
430 120 C for 20 minutes. The gold electrodes were then thermally evaporated onto the perovskite
431 films through a shadow mask. Then polymethylmethacrylate (PMMA) (20 mg/ml) or PCBM (20

432 mg/ml) or Spiro-OMeTAD (100 mg/ml) were spin coated on to the perovskite films at 2000 rpm
433 for 45 seconds.

434 For the PbAc₂ derived perovskite films, 1M solutions of 3:1 MAI:PbAc₂ with or without .0075M
435 hypophosphorous acid were spin coated at 2000 rpm for 45 seconds. The films were allowed to
436 sit at room temperature for 5 minutes, after which they were annealed at 100 C for 5 minutes.

437 *Steady State photocurrent measurements*

438 Samples were illuminated with a mechanically chopped laser source (either 650 or 850 as
439 detailed in the main text). A power supply was used to provide a voltage bias across the devices
440 and the current was recorded on a lock-in amplifier in current mode, set to the chopping
441 frequency. The chopping frequency was set to 23 Hz.

442 In the case where a visible light bias was used and only the sub gap contribution measured, a 690
443 nm laser was continuously illuminating the samples while a mechanically chopped 850 nm laser
444 excitation was used to detect the subgap contribution. Again, the modulated photocurrent was
445 detected with a lock-in amplifier. In all cases the laser excitation was defocused to cover the
446 entire area between the electrodes. The noise at the output of the lock-in used here (SR530) is
447 $0.13 \text{ pA}/\sqrt{\text{Hz}}$ and with a specified bandwidth of 0.01Hz, we have a noise level of 6fA. This
448 gives more than enough room to measure the pA signals which were the lowest reported in this
449 work.

450

451 Excitation density was estimated by assuming that 90 % of the above gap excitation was
452 absorbed within the perovskite. The red excitation was used to ensure a fairly uniform absorption
453 profile, and for the sake of simplicity, the total generated carriers were assumed to be uniformly
454 distributed throughout the bulk.

455 *Transient Photocurrent Spectroscopy*

456 The same samples were excited by 1 ns laser pulses (690 nm, 1 Hz repetition rate), making sure
457 to illuminate the entire area between the electrodes. A power supply was used to bias the sample,
458 while the photocurrent was amplified with a trans-impedance amplifier (gain X 10,000) and then
459 measured with an oscilloscope.

460 To confirm that we are not simply measuring the time for carrier to be swept out by the electric
461 field, we calculate the sweep-out time using a mobility of $20 \text{ cm}^2 \text{ V}^{-1} \text{ s}^{-1}$ as an upper limit. This
462 yields a lower limit sweep out time of 8 ms, far longer than any of the events we have described
463 above.

464 *Transient Absorption Spectroscopy*

465 Transient absorption (TA) spectroscopy was conducted using an amplified Ti:sapphire laser (100
466 fs pulses at 800 nm) focused into a sapphire plate to generate a broadband white light probe. The
467 frequency-doubled output of a Q-switched Nd:YVO₄ laser acted as a pump (700 ps FWHM
468 pulses at 532 nm), synchronized to the Ti:sapphire laser *via* a digital delay generator. This setup
469 enables us to perform TA over pump-probe delays from one nanosecond to hundreds of
470 microseconds, covering the timescales of both band-to-band recombination and long lived trap
471 recombination.

472

473 *FTPS*

474 Fourier transform photocurrent spectroscopy was performed by using a modified FTIR setup.
475 The excitation was focused onto the perovskite device which was biased by an external power
476 supply. The photocurrent was amplified, recorded, and the interferogram converted to a
477 photocurrent spectrum by a custom designed program.

478 **Acknowledgements**

479 The authors acknowledge the funding from the EU Seventh Framework Program [FP7/2007-203]
480 under grant agreement number 604032 of the MESO project and DESTINY Marie-Curie
481 network under grant agreement number 316494.

- 482 1. NREL. Best Research-Cell Efficiencies. at
483 <http://www.nrel.gov/ncpv/images/efficiency_chart.jpg>
- 484 2. Jeon, N. J. *et al.* Compositional engineering of perovskite materials for high-performance
485 solar cells. *Nature* **517**, Advance (2015).
- 486 3. Atsuhiko Miyata, Anatolie Mitioğlu, Paulina Plochocka, Oliver Portugall, Jacob Tse-Wei
487 Wang, Samuel D. Stranks, Henry J. Snaith, and R. J. N. Direct Measurement of the
488 Exciton Binding Energy and Effective 1 Masses for Charge carriers in an Organic-
489 Inorganic Tri-halide Perovskite. *Nat. Phys.*
- 490 4. D’Innocenzo, V. *et al.* Excitons versus free charges in organo-lead tri-halide perovskites.
491 *Nat Commun* **5**, 3586 (2014).
- 492 5. Stranks, S. D. *et al.* Electron-Hole Diffusion Lengths Exceeding 1 Micrometer in an
493 Organometal Trihalide Perovskite Absorber. *Science* (80-.). **342**, 341–344 (2013).
- 494 6. Xing, G. *et al.* Long-range balanced electron- and hole-transport lengths in organic-
495 inorganic CH₃NH₃PbI₃. *Science* **342**, 344–7 (2013).
- 496 7. Wehrenfennig, C., Eperon, G. E., Johnston, M. B., Snaith, H. J. & Herz, L. M. High
497 Charge Carrier Mobilities and Lifetimes in Organolead Trihalide Perovskites. *Adv. Mater.*
498 **26**, 1584–1589 (2013).
- 499 8. De Wolf, S. *et al.* Organometallic Halide Perovskites: Sharp Optical Absorption Edge and
500 its Relation to Photovoltaic Performance. *J. Phys. Chem. Lett.* **5**, 1035–1039 (2014).
- 501 9. Stranks, S. D. *et al.* Electron-Hole Diffusion Lengths Exceeding. **342**, 341–344 (2013).
- 502 10. Stranks, S. D. *et al.* Recombination Kinetics in Organic-Inorganic Perovskites: Excitons,
503 Free Charge, and Subgap States. *Phys. Rev. Appl.* **2**, 34007 (2014).
- 504 11. Yamada, Y., Nakamura, T., Endo, M., Wakamiya, A. & Kanemitsu, Y. Photocarrier
505 Recombination Dynamics in Perovskite CH₃NH₃PbI₃ for Solar Cell Applications. *J. Am.*
506 *Chem. Soc.* **136**, 11610–11613 (2014).

- 507 12. Tan, Z.-K. *et al.* Bright light-emitting diodes based on organometal halide perovskite. *Nat.*
508 *Nanotechnol.* 1–6 (2014). doi:10.1038/nnano.2014.149
- 509 13. Deschler, F. *et al.* High Photoluminescence Efficiency and Optically Pumped Lasing in
510 Solution-Processed Mixed Halide Perovskite Semiconductors. *J. Phys. Chem. Lett.* 1421–
511 1426 (2014). doi:10.1021/jz5005285
- 512 14. Zhu, H. *et al.* Lead halide perovskite nanowire lasers with low lasing thresholds and high
513 quality factors. *Nat. Mater.* (2015).
- 514 15. Leijtens, T. *et al.* Electronic properties of meso-superstructured and planar organometal
515 halide perovskite films: charge trapping, photodoping, and carrier mobility. *ACS Nano* **8**,
516 7147–7155 (2014).
- 517 16. Wu, X. *et al.* Trap States in Lead Iodide Perovskites. *J. Am. Chem. Soc.* (2015). at
518 <<http://dx.doi.org/10.1021/ja512833n>>
- 519 17. Ponseca, C. S. *et al.* Organometal Halide Perovskite Solar Cell Materials Rationalized:
520 Ultrafast Charge Generation, High and Microsecond-Long Balanced Mobilities, and Slow
521 Recombination. *J. Am. Chem. Soc.* **136**, 5189 – 5192 (2014).
- 522 18. Shockley, W. & Read, W. T. Statistics of the Recombinations of Holes and Electrons.
523 *Phys. Rev.* **87**, 835–842 (1952).
- 524 19. Palomares, E. J., Marin-Beloqui, J. M. & Perez Hernandez, J. Photo-Induced Charge
525 Recombination Kinetics in MAPbI₃-xCl_x Perovskite-like Solar Cells Using Low Band-
526 Gap Polymers as Hole Conductors. *Chem. Commun.* **50**, 14566–14569 (2014).
- 527 20. Stranks, S. D. *et al.* Electron-hole diffusion lengths exceeding 1 micrometer in an
528 organometal trihalide perovskite absorber. *Science* **342**, 341–4 (2013).
- 529 21. Bi, D. *et al.* Efficient luminescent solar cells based on tailored mixed-cation perovskites.
530 *Sci. Adv.* **2**, (2016).
- 531 22. Baena, J. P. C. *et al.* Highly efficient planar perovskite solar cells through band alignment
532 engineering. *Energy Environ. Sci.* **8**, 2928–2934 (2015).
- 533 23. Filippetti, A., Delugas, P. & Mattoni, A. Radiative Recombination and Photoconversion of
534 Methylammonium Lead Iodide Perovskite by First Principles: Properties of an Inorganic
535 Semiconductor within a Hybrid Body. *J. Phys. Chem. C* **118**, 24843–24853 (2014).
- 536 24. Leijtens, T. *et al.* Mapping Electric Field – Induced Switchable Polarization and Structural
537 Degradation in Hybrid Lead Halide Perovskite Thin Films. *Adv. Energy Mater.*
538 10.1002/aenm.201500962 (2015). doi:10.1002/aenm.201500962

- 539 25. Trapping, C. *et al.* Electronic Properties of Meso-Superstructured and Planar Organometal
540 Halide Perovskite Films : (2014).
- 541 26. Pathak, S. *et al.* Atmospheric Influence upon Crystallization and Electronic Disorder and
542 Its Impact on the Photophysical Properties of Organic-Inorganic Perovskite Solar Cells.
543 (2015).
- 544 27. Yin, W.-J., Shi, T. & Yan, Y. Unusual defect physics in CH₃NH₃PbI₃ perovskite solar
545 cell absorber. *Appl. Phys. Lett.* **104**, 063903 (2014).
- 546 28. Du, M.-H. Density Functional Calculations of Native Defects in CH₃NH₃PbI₃: Effects of
547 Spin–Orbit Coupling and Self-Interaction Error. *J. Phys. Chem. Lett.* **6**, 1461–1466
548 (2015).
- 549 29. Borriello, I., Cantele, G. & Ninno, D. Ab initio investigation of hybrid organic-inorganic
550 perovskites based on tin halides. *Phys. Rev. B* **77**, 235214 (2008).
- 551 30. Rose, A. *Concepts in photoconductivity and allied problems.* (Interscience publishers,
552 1963).
- 553 31. Shao, Y., Yuan, Y. & Huang, J. Correlation of energy disorder and open-circuit voltage in
554 hybrid perovskite solar cells. *Nat. Energy* **1**, 15001 (2016).
- 555 32. Giorgi, G., Fujisawa, J.-I., Segawa, H. & Yamashita, K. Small Photocarrier Effective
556 Masses Featuring Ambipolar Transport in Methylammonium Lead Iodide Perovskite: A
557 Density Functional Analysis. *J. Phys. Chem. Lett.* **4**, 4213–4216 (2013).
- 558 33. Filippetti, A., Mattoni, A., Caddeo, C., Saba, M. I. & Delugas, P. Low electron-polar
559 optical phonon scattering as a fundamental aspect of carrier mobility in methylammonium
560 lead halide CH₃NH₃PbI₃ perovskites. *Phys. Chem. Chem. Phys.* **18**, 15352–15362
561 (2016).
- 562 34. DeQuilettes, D. W. *et al.* Impact of microstructure on local carrier lifetime in perovskite
563 solar cells. *Science (80-)*. (2015). doi:10.1126/science.aaa5333
- 564 35. O'Regan, B. C. *et al.* Opto-electronic studies of methylammonium lead iodide perovskite
565 solar cells with mesoporous TiO₂; separation of electronic and chemical charge storage,
566 understanding two recombination lifetimes, and the evolution of band offsets during JV
567 hysteresis. *J. Am. Chem. Soc.* 150318153052006 (2015). doi:10.1021/jacs.5b00761
- 568 36. Eppler, A. M., Ballard, I. M. & Nelson, J. Charge transport in porous nanocrystalline
569 titanium dioxide. in *Phys. E Low-Dimensional Syst. Nanostructures* **14**, 197–202 (2002).
- 570 37. Lakhwani, G. *et al.* Probing charge carrier density in a layer of photodoped ZnO
571 nanoparticles by spectroscopic ellipsometry. *J. Phys. Chem. C* **114**, 14804–14810 (2010).

- 572 38. Yin, W., Yang, J., Kang, J., Yan, Y. & Wei, S.-H. Halide Perovskite Materials for Solar
573 Cells: A Theoretical Review. *J. Mater. Chem. A* In Press (2015).
574 doi:10.1039/C4TA05033A
- 575 39. Walsh, A., Scanlon, D. O., Chen, S., Gong, X. G. & Wei, S.-H. Self-Regulation
576 Mechanism for Charged Point Defects in Hybrid Halide Perovskites. *Angew. Chemie Int.*
577 *Ed.* **54**, 1791–1794 (2015).
- 578 40. Manser, J. S. & Kamat, P. V. Band filling with free charge carriers in organometal halide
579 perovskites. *Nat. Photonics* **8**, 737–743 (2014).
- 580 41. Zhang, W. *et al.* Ultrasmooth organic–inorganic perovskite thin-film formation and
581 crystallization for efficient planar heterojunction solar cells. *Nat. Commun.* **6**, 6142
582 (2015).
- 583 42. Zhang, W. *et al.* Enhanced optoelectronic quality of perovskite thin films with
584 hypophosphorous acid for planar heterojunction solar cells. *Nat Commun* **6**, (2015).
- 585 43. Zhang, W. *et al.* Ultrasmooth organic-inorganic perovskite thin-film formation and
586 crystallization for efficient planar heterojunction solar cells. *Nat Commun* **6**, 6142 (2015).
- 587 44. Eperon, G. E., Burlakov, V. M., Docampo, P., Goriely, A. & Snaith, H. J. Morphological
588 control for high performance, solution-processed planar heterojunction perovskite solar
589 cells. *Adv. Funct. Mater.* **24**, 151–157 (2014).
- 590 45. Kittel, C. & Holcomb, D. F. Introduction to solid state physics. *Am. J. Phys.* **35**, 547–548
591 (1967).
- 592 46. Tvingstedt, K. *et al.* Radiative efficiency of lead iodide based perovskite solar cells. *Nat.*
593 *Sci. Reports* **4**, 1–7 (2014).
- 594